

# Can Image Splicing and Copy-Move Forgery Be Detected by the Same Model?

## Forensim: An Attention-Based State-Space Approach

Soumyaroop Nandi<sup>1,2</sup> Prem Natarajan<sup>1,2</sup>

<sup>1</sup>USC Information Sciences Institute, Marina del Rey, CA, USA

<sup>2</sup>USC Thomas Lord Department of Computer Science, Los Angeles, CA, USA

{soumyarn, premkunn}@usc.edu

### Abstract

We introduce *Forensim*, an attention-based state-space framework for image forgery detection that jointly localizes both manipulated (target) and source regions. Unlike traditional approaches that rely solely on artifact cues to detect spliced or forged areas, *Forensim* is designed to capture duplication patterns crucial for understanding context. In scenarios like protest imagery, detecting only the forged region—e.g., a duplicated act of violence inserted into a peaceful crowd—can mislead interpretation, highlighting the need for joint source-target localization. *Forensim* outputs three-class masks (pristine, source, target) and supports detection of both splicing and copy-move forgeries within a unified architecture. We propose a visual state-space model that leverages normalized attention maps to identify internal similarities, paired with a region-based block-attention module to distinguish manipulated regions. This design enables end-to-end training and precise localization. *Forensim* achieves state-of-the-art performance on standard benchmarks. We also release CMFDAnything, a new dataset addressing limitations of existing copy-move forgery datasets. [Project page and code](#).

### 1. Introduction

The proliferation of generative models has broadened image manipulation far beyond traditional editing tools. The challenge for today’s researchers is to detect manipulated images, irrespective of the source of manipulation, be it generative models [13, 22, 29, 33, 52], tampered with by photo editing tools [9, 32, 40] or online social media filters [45]. Deceitful attackers may spread misinformation in the form of internet rumors [45], fake news [19], deep fakes [34, 36], forged satellite images [18] plagiarized academic publications [35, 36]. The prediction of the source of manipulation in the tampered images would be a vital contribution to the image manipulation detection community. Without the knowledge of the source of manipulation,

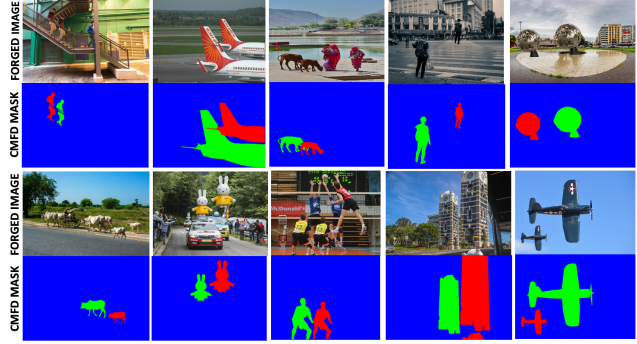


Figure 1. Proposed CMFDAnything samples- Rows show: (a) forged image, (b) RGB mask, (c) forged image, (d) RGB mask. Source-target mask encodes `untampered`, `source`, & `target` regions.

tracing a tampered image becomes a challenging task.

Tracing the source of image manipulation is possible if a model is trained to detect all forms of image tampering, whether involving image content or not. Image content-based forgeries can originate externally, where patches from an unrelated image are inserted (*splicing forgery*), or internally, where parts of the same image are duplicated and repositioned (*copy-move forgery*). Some forgers attempt to remove objects or regions from an image and seamlessly replace them with background pixels (*inpainting forgery*).

Beyond direct content manipulation, images can also be subtly altered without modifying their content through various forms of *image enhancement*, such as quantization, noise addition, resampling, blurring, morphing, compression, and histogram manipulation. Additionally, image tampering can stem from generative model-based synthesis [6, 42] or transformations introduced by social media [45].

However, prior research has predominantly approached forgery detection from the perspective of image splicing, where models are trained with binary masks to capture artifact cues near manipulated regions. These approaches often assume that techniques effective for splicing generalize well

to all types of manipulation, including copy-move forgeries. Traditional splicing detection models localize only the manipulated regions, without accounting for the duplicated source regions. In contrast, our proposed model, Forensim, is trained using three-class masks—**pristine**, **source**, and **target**—to handle both splicing and copy-move forgeries in a unified framework, as illustrated in [Fig. 5](#).

For example, in a forensic investigation, establishing a crime often requires not only identifying the manipulated evidence—such as perpetrator’s fingerprints—but also tracing its origin, such as matching the fingerprint in a database. Analogously, in image manipulation detection and localization (IMDL), detecting a tampered region without locating its source can be insufficient, particularly when both exist within the same image. This observation motivates our approach, which reformulates the image forgery detection task as a three-class mask segmentation problem. Our framework is capable of distinguishing all relevant regions, and experimental results demonstrate that this design generalizes effectively across both image splicing/inpainting scenarios (binary masks) and copy-move forgery detection (CMFD), offering improved interpretability and robustness.

In this paper, we introduce a novel state-space model-based attention mechanism designed to accurately localize both the source and forged regions in IMDL. Specifically, we propose a similarity (Sim\_Attn) and manipulation (MSSA) attention modules, both of which leverage image affinity matrices to guide attention-based learning. Sim\_Attn identifies and highlights similar regions within an image, while MSSA distinguishes forged regions from naturally occurring identical patterns. By jointly learning these complementary attention mechanisms, our approach effectively mitigates misdetections and false alarms, addressing the key limitations of existing IMDL models.

The attention modules efficiently capture long-range dependencies while maintaining linear computational complexity and low memory usage. Additionally, we normalize the attention weights in the discretization step of the Mamba formulation in [Eq.2](#). This normalization ensures a well-balanced distribution of attention, enhancing robustness—particularly in fine-grained tasks such as CMFD. Furthermore, we have conducted extensive experiments with different MSSA blocks in [Fig.4](#) to develop a robust and effective CMFD architecture.

Training deep learning models for CMFD requires synthetic datasets, as open-source CMFD datasets are scarce. To address this, we introduce CMFDAnything, a benchmark dataset derived from high-quality SegmentAnything images [\[23\]](#). Existing CMFD datasets, often created from MSCOCO [\[26\]](#), are limited and contain forgeries that are easily detectable by the naked eye. In contrast, CMFDAnything generates realistic, high-quality forgeries, enabling the development of robust models like Forensim to

detect highly post-processed tampered images in [Fig.1](#).

To unify splicing and CMFD, Forensim is trained on both spliced images with binary masks and CMFD images with source-target masks, enabling generalization across manipulation types. Our key contributions are:

- We reformulate IMDL as a three-class training task, enabling unified detection of both CMFD and splicing forgeries—unlike prior work limited to binary-mask training focused on artifact-based splicing detection.
- We propose similarity and manipulation attention modules within a state-space framework that effectively capture long-range dependencies with linear complexity.
- We introduce CMFDAnything, a high-resolution copy-move forgery dataset derived from Segment Anything images, and demonstrate Forensim’s state-of-the-art performance on multiple CMFD benchmarks.

## 2. Related Work

### 2.1. Earlier IMDL Methods

Handcrafted feature-based methods for Image Manipulation Detection and Localization (IMDL) include ELA [\[24\]](#) (detects compression error differences between forged and pristine regions), NOI1 [\[28\]](#) (models local noise using high-pass wavelet coefficients), and CFA1 [\[12\]](#) (approximates camera filter array patterns). These methods typically focus on splicing detection. Early DNN-based studies also targeted specific forgeries, such as splicing [\[8\]](#), copy-move [\[7\]](#), removal [\[54\]](#), and enhancement [\[2\]](#). However, real-world manipulated images lack prior information about the forgery type, motivating the development of general forgery detection algorithms that can identify any manipulation.

### 2.2. Image Splicing Models and Training Datasets

Most image splicing frameworks consist of an input feature extraction network, feature fusion (if multiple artifacts), and an anomaly detection network that classifies each pixel as tampered or pristine to generate a binary localization map. These networks are typically pre-trained on synthetic datasets, like MS-COCO [\[26\]](#). ManTraNet [\[47\]](#) detects 385 manipulation types using a bipartite end-to-end network but struggles with double JPEG compression artifacts. MVSS-Net [\[3\]](#) uses noise distribution for feature generalization but fails to balance sensitivity and specificity. CAT-Net [\[25\]](#) focuses on compression artifacts and is designed for image splicing only. IF-OSN [\[45\]](#) addresses artifacts from online social networks but struggles with traditional IMDL models. Trufor [\[16\]](#) generates manipulation and confidence maps but does not predict manipulation sources. HiFi-Net [\[17\]](#) treats IMDL as a multi-level classification task but fails when similar copy-move regions are present. None of these methods predict the source of manipulation, struggling in scenarios with similar copy-move regions.

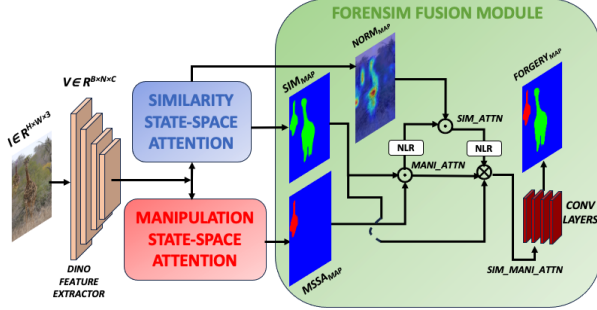


Figure 2. Forensim Overview: Sim-Mani Attention and Fusion

### 2.3. CMFD Models and Training Datasets

BusterNet [46] is the first end-to-end deep neural network for CMFD, featuring dual branches for source-target localization and trained on the synthetic USC-ISI CMFD dataset derived from MSCOCO [26] and SUN2012 [48]. DOA-GAN [20] similarly adopts a GAN-based framework trained on the same dataset. However, both models struggle with complex copy-move forgeries and fail to generalize to image splicing, exhibiting high false alarm and misdetection rates, as shown in Fig. 6. The limited diversity, low complexity, and lack of availability of the USC-ISI dataset motivated us to develop the CMFD Anything dataset.

### 2.4. Structured State Space Models

Structured state space models (SSM) offer an alternative to Transformer and CNN-based models, modeling long-range dependencies with linear scaling in sequence length. Recent advancements, such as S4 [15] and Mamba [14], utilize structured SSMs for efficient long-range dependency modeling. VisionMamba [53] and VMamba [27] further extend this for computer vision tasks. Despite their success, these models often lack task-specific design considerations, especially in IMDL. Our approach leverages a specialized SSM design optimized for similarity and manipulation detection, achieving better accuracy with lower complexity.

## 3. Proposed Method

### 3.1. State Space Model Overview

State Space Models (SSMs) [14, 15, 27] are linear time-invariant (LTI) systems that effectively capture complex sequential dependencies, similar to the Kalman Filter [21], which is designed for linear systems with simple dynamics. Given a continuous input sequence  $x(t) \in \mathbb{R}$ , the system produces a continuous output  $y(t) \in \mathbb{R}$  through a hidden state  $h(t) \in \mathbb{R}^N$ . The system's evolution is governed by the parameter  $\mathbf{A} \in \mathbb{R}^{N \times N}$ , while  $\mathbf{B} \in \mathbb{R}^{N \times 1}$  and  $\mathbf{C} \in \mathbb{R}^{1 \times N}$  act as projection parameters. The continuous system follows these governing equations:

$$h'(t) = \mathbf{A}h(t) + \mathbf{B}x(t)$$

$$y(t) = \mathbf{C}h(t)$$

A timescale parameter  $\Delta$  is used to transform the continuous parameters  $\mathbf{A}$ ,  $\mathbf{B}$  into their discrete counterparts, denoted as  $\bar{\mathbf{A}}$ ,  $\bar{\mathbf{B}}$ , as described in [14, 15]. A widely adopted approach for this transformation is the zero-order hold (ZOH) [15], which is defined as follows:

$$\begin{aligned} \bar{\mathbf{A}} &= \exp(\Delta \mathbf{A}), \quad \bar{\mathbf{B}} = (\Delta \mathbf{A})^{-1} (\exp(\mathbf{A}) - \mathbf{I}) \Delta \mathbf{B}, \quad \bar{\mathbf{C}} = \mathbf{C}, \\ y_k &= \bar{\mathbf{C}}h_k + \bar{\mathbf{D}}x_k, \\ h_k &= \bar{\mathbf{A}}h_{k-1} + \bar{\mathbf{B}}x_k \end{aligned} \quad (1)$$

$\bar{\mathbf{D}}$  works as a residual connection and  $\bar{\mathbf{B}}$  can be approximated using the first-order Taylor series as:

$$\bar{\mathbf{B}} = (\exp(\mathbf{A}) - \mathbf{I}) \mathbf{A}^{-1} \mathbf{B} \approx (\Delta \mathbf{A})(\Delta \mathbf{A})^{-1} \Delta \mathbf{B} = \Delta \mathbf{B}$$

**Selective Scan:** Mamba [14] excels at capturing and modeling complex interactions in long sequences through a selective scanning mechanism. The matrices  $\mathbf{B} \in \mathbb{R}^{L \times N}$ ,  $\mathbf{C} \in \mathbb{R}^{L \times N}$ , and  $\Delta \in \mathbb{R}^{L \times D}$  are computed from the input  $\mathbf{x} \in \mathbb{R}^{L \times D}$ , enabling the model to preserve contextual awareness. While this approach removes invariant parameters in one-dimensional temporal inputs, such as text, the 2D-Selective scan in VMamba [27] extends this capability to two-dimensional images by incorporating spatial information and non-sequential structures through the Visual State Space Block (VSSM).

In the first step, Cross-Scan, VSSM flattens input patches into four sequences, each following a distinct state space trajectory. Each sequence is processed independently and in parallel by separate VSSM instances to effectively capture long-range dependencies, as described in (Eqs. 1, 2). Finally, in the Cross-Merge step, the processed sequences are reshaped and combined, generating an output map with global receptive fields in the two-dimensional space.

### 3.2. Forensim Overview

The architecture of the Forensim model is illustrated in Fig. 2. It is specifically designed for three-class supervised forgery detection, employing state-space-based feature extraction and attention mechanisms to improve forgery localization. Given an input image  $I \in \mathbb{R}^{H \times W \times 3}$ , the model utilizes the first four layers of an ImageNet-pretrained Vision Transformer backbone (DINO) to extract high-dimensional hierarchical feature representations  $V \in \mathbb{R}^{B \times N \times C}$ , where  $B$  is the batch size,  $N = H \times W$ , and  $C = 384$  represents the embedding dimension for our proposed Similarity Attention Module. These features are subsequently flattened and processed through the proposed Similarity State Space Attention module, which constructs an affinity matrix  $Aff \in \mathbb{R}^{N \times N}$  by capturing self-similarity patterns within the image. This mechanism enhances the detection of duplicated regions, aiding in forgery identification.

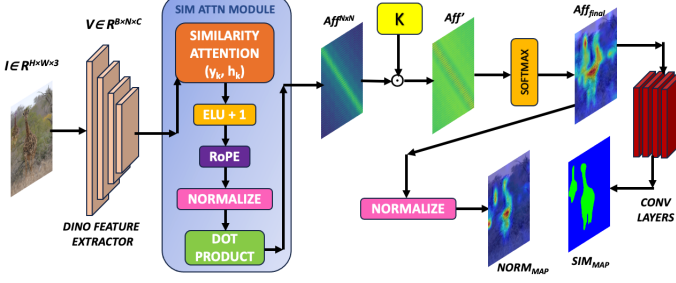


Figure 3. Similarity State Space Attention Module

### 3.3. Similarity State Space Attention Module

Given an extracted feature map  $V \in \mathbb{R}^{B \times N \times C}$ , the module computes an explicit affinity matrix  $Aff \in \mathbb{R}^{N \times N}$  that captures the similarity between different spatial locations, as shown in Fig.3. Leveraging the State Space Similarity mechanism described in Eq. 1, we normalize  $\bar{C}h_k$  such that:

$$\begin{aligned} y_k &= \bar{C}h_k / \bar{C}n_k + \bar{D}x_k, \\ h_k &= \bar{A}h_{k-1} + \bar{B}x_k \end{aligned} \quad (2)$$

Here,  $h_k = \sum_{j=1}^k \bar{B}_j^\top x_j$  and  $n_k = \sum_{j=1}^k \bar{B}_j$  [14]. Eq.2 defines the similarity attention with a global receptive field. Given a token  $k$  and its preceding token  $j$ , where  $j \leq k$ , each  $\bar{A}$  aggregates information from all  $x_k$  and  $y_k$ . Similarity Attention divides the output by  $\bar{C}n_k$ , to ensure that the attention weights sum up to 1.

We incorporate Rotary Positional Embeddings (RoPE) [37] into the similarity attention mechanism to ensure that the affinity matrix captures spatial dependencies across the image effectively. Additionally, an ELU activation function is applied to  $V_k$  prior to normalization to enhance stability during similarity computation. The Similarity Attention module computes an explicit affinity matrix via a dot product between the transformed representations  $\bar{C}$  and  $\bar{B}$ , as defined in Eq. 2. Given an input  $V \in \mathbb{R}^{B \times N \times C}$ , the vectors  $\bar{C}$  and  $\bar{B}$  are computed as:

$$\bar{C}, \bar{B} = \text{ELU}(\text{Linear}(V_k)) + 1.0 \quad (3)$$

These features are subsequently modulated using RoPE. Specifically, they are reshaped, augmented with rotary positional encoding, and then normalized as follows:

$$\bar{C} = \frac{\text{RoPE}(\bar{C})}{\|\bar{C}\|_2}, \quad \bar{B} = \frac{\text{RoPE}(\bar{B})}{\|\bar{B}\|_2} \quad (4)$$

Finally, the explicit affinity matrix is computed using the dot product between the modulated feature representations:

$$Aff = \bar{C}\bar{B}^\top, \quad Aff \in \mathbb{R}^{B \times N \times N} \quad (5)$$

This yields a structured affinity representation that captures spatial relationships and preserves computational efficiency.

When calculating the similarity attention of an image, the affinity matrix  $Aff$  exhibits higher values along the diagonal, as these values represent the correlation of a region

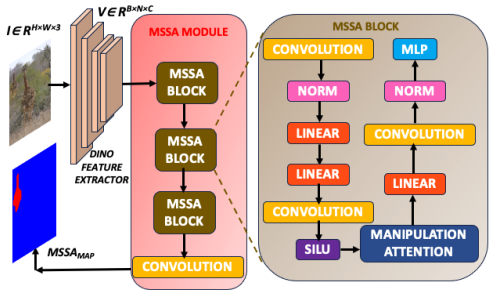


Figure 4. Manipulation State Space Attention Module

with itself. To resolve this issue, we define an operation  $K$ , as follows:

$$K(p, q, p', q') = \frac{(p - p')^2 + (q - q')^2}{(p - p')^2 + (q - q')^2 + \sigma^2} \quad (6)$$

We obtain a new affinity matrix  $Aff' = Aff \odot K$ , where  $\odot$  denotes the element-wise dot product.

To refine the affinity matrix, a bidirectional softmax operation is applied, ensuring that the final similarity values are mutually reinforced between spatial locations by utilizing the patch-matching strategy from [4], we compute the likelihood that a patch in the  $p$ -th row matches with a patch in the  $q$ -th column of  $Aff'$  to compute the final affinity matrix  $Aff_{final}$  as follows:

$$Aff_{row}(p, q) = \frac{\exp(\alpha Aff'[p, q])}{\sum_{q'=1}^N \exp(\alpha Aff'[p, q'])}, \quad (7)$$

$$Aff_{col}(p, q) = \frac{\exp(\alpha Aff'[p, q])}{\sum_{p'=1}^N \exp(\alpha Aff'[p', q])}, \quad (8)$$

$$Aff_{final}(p, q) = Aff_{row}(p, q) \cdot Aff_{col}(p, q). \quad (9)$$

Here,  $\alpha$  is a hyperparameter, set to 5. The final affinity matrix  $Aff_{final} \in \mathbb{R}^{N \times N}$  is then refined using a Convolutional module, which comprises four convolutional layers followed by a SiLU activation. These layers process the affinity matrix to generate the similarity attention map  $Sim_{map} \in \mathbb{R}^{\sqrt{N} \times \sqrt{N}}$ , which highlights the top-k most similar regions per pixel.

We also obtain a normalized affinity map  $Norm_{map} \in \mathbb{R}^{N \times \sqrt{N} \times \sqrt{N}}$  from Eq.6 to capture spatial dependencies across the entire image, such that:

$$\text{Norm}_{Map}(p, q) = \frac{(Aff_{final}(p, q))}{\left(\sum_{q'=1}^N Aff_{final}(p, q')\right)} \quad (10)$$

### 3.4. Manipulation State Space Attention Module

The Multi-Level Manipulation State Space Attention (MSSA) module enhances tampered region detection by using a multi-scale state space attention mechanism composed

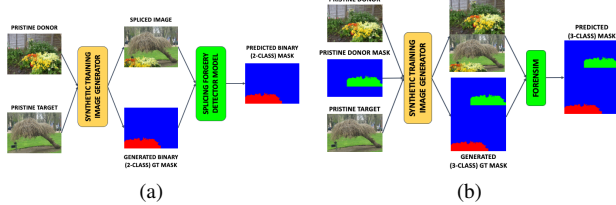


Figure 5. Splicing Training: (a) Baselines supervise only with target masks. (b) Forensim uses both source and target masks.

of three  $MSSA_{Block}$  units. Each block processes the input with a specified number of attention heads to capture both global context and local feature details, addressing the computational challenges of traditional self-attention methods for high-resolution images.

Given an extracted feature  $V \in \mathbb{R}^{B \times N \times C}$ , the three  $MSSA$  blocks capture multi-scale information, and their outputs are averaged and reshaped to the original spatial dimensions. A final convolution layer followed by SiLU activation produces the  $MSSA_{map}$ , which highlights potential forgery regions while suppressing background noise, as illustrated in Fig. 4.

Manipulation Attention in Fig.4 incorporates Locally Enhanced Positional Encoding (LePE) [11] and Rotary Position Embedding (RoPE) [37] to enhance spatial awareness. Given an extracted input  $V \in \mathbb{R}^{B \times N \times C}$ , the  $\bar{\mathbf{C}}$  and  $\bar{\mathbf{B}}$  from Eq.2 are computed as:

$$\bar{\mathbf{C}}, \bar{\mathbf{B}} = \text{ELU}(\text{Linear}(V_k)) + 1.0 \quad (11)$$

The representation is further modulated using RoPE, and attention is computed efficiently as:

$$p = \frac{1}{\bar{\mathbf{C}}\bar{\mathbf{B}}^\top + \epsilon}, \quad \bar{\mathbf{B}}V_k = (\bar{\mathbf{B}}^\top N^{-0.5})(V_k N^{-0.5}) \quad (12)$$

$$V_k = (\bar{\mathbf{C}} \cdot \text{RoPE}(\bar{\mathbf{B}}))\bar{\mathbf{B}}V_k \cdot p + \text{LePE}(V_k) \quad (13)$$

Local Positional Encoding (LePE), implemented via depth-wise convolution, enhances local feature aggregation and improves representational capacity. The generated  $V_k$  is passed through a combination of linear, CPE, normalization, and MLP layers to produce the  $MSSA$  Block output.

The  $MSSA_{Block}$  comprises a convolutional patch embedding (CPE) layer, normalization layers, and multi-head attention mechanisms. It sequentially applies convolution, normalization, and SiLU activation, followed by the manipulation state-space attention mechanism defined in Eq. 2, and a feed-forward network (MLP). Residual connections and drop path regularization further refine the output, enabling the  $MSSA$  Block to capture fine-grained spatial patterns for tampered region detection while maintaining computational efficiency.

Table 1. Image Quality Assessment (IQA) on CMFD datasets.  $\uparrow$  indicates higher is better;  $\downarrow$  indicates lower is better.

Method	Type	CASIA CMFD [10]	CoMoFoD [39]	CMFD Anything
PaQ-2-PiQ [49] ( $\uparrow$ )	No-Ref	3.64	3.42	<b>4.11</b>
CLIP-IQA [41] ( $\uparrow$ )	No-Ref	6.58	6.42	<b>7.23</b>
SSIM [43] ( $\uparrow$ )	Full-Ref	0.832	0.779	<b>0.881</b>
LPIPS [51] ( $\downarrow$ )	Full-Ref	0.179	0.243	<b>0.124</b>

### 3.5. Forensim Fusion Module

To efficiently integrate extracted features, we propose a Non-Local Refinement (NLR) module that propagates information across spatial locations using the similarity map  $\text{Sim}_{\text{map}}$  and normalization map  $\text{Norm}_{\text{map}}$  from Section 3.3, along with the manipulation self-structure attention map  $MSSA_{\text{map}}$  from Section 3.4. This operation enhances contextual coherence by reinforcing semantically meaningful regions and suppressing irrelevant background signals. We formalize the NLR operation as a non-local weighted aggregation of features:

$$\text{NLR}(F)_i = \sum_j A_{ij} \cdot F_j, \quad A_{ij} = \frac{\exp(S_{ij})}{\sum_k \exp(S_{ik})} \quad (14)$$

where  $F \in \mathbb{R}^{C \times N}$  is the input feature map,  $S_{ij}$  is the similarity between locations  $i$  and  $j$ , and  $A_{ij}$  is the softmax-normalized attention weight. This operation allows each spatial feature to integrate context from semantically related regions, guided by similarity and manipulation cues.

We apply this refinement to both the manipulation and similarity attention pathways as follows:

$$\text{Mani\_Attn} = \text{NLR}(\text{MSSA}_{\text{map}} \odot \text{Sim}_{\text{map}}) \quad (15)$$

$$\text{Sim\_Attn} = \text{NLR}(\text{Mani\_Attn} \odot \text{Norm}_{\text{map}}) \quad (16)$$

where  $\odot$  denotes the Hadamard product.

We then construct the fused representation  $\text{Sim\_Mani\_Attn} \in \mathbb{R}^{C \times \sqrt{N} \times \sqrt{N}}$  by channel-wise concatenating the aggregated features, as illustrated in Fig. 2:

$$\text{Sim\_Mani\_Attn} = \text{Mani\_Attn} \otimes \text{Sim\_Attn} \otimes \text{Sim}_{\text{map}} \quad (17)$$

where  $\otimes$  denotes channel-wise concatenation.

This fused representation captures global self-similarity, local manipulation context, and fine-grained structural cues. It is further processed by a sequence of convolutional layers with SiLU activations (as described in Section 3.3) to produce a pixel-level forgery mask and an image-level detection score. This structured design enables Forensim to generalize robustly across diverse manipulation types through context-aware, semantically aligned feature integration.

## 4. Training and Implementation

### 4.1. Image Splicing using CMFD Training Setup

Forensim is designed to detect both splicing and copy-move forgeries using a unified architecture that outputs 3-class

Methods	Precision (Localization)			Recall (Localization)			F1 (Localization)			AUC	Precision	Recall	F1
	P	S	T	P	S	T	P	S	T				
<b>USC-ISI CMFD Test Set [46]</b>													
BusterNet [46]	93.71	55.85	53.84	99.01	38.26	48.73	96.15	40.84	48.33	0.64	89.26	80.14	84.45
ManTra-Net [47]	93.50	8.66	48.53	<u>99.22</u>	2.28	28.43	96.08	2.97	30.58	0.53	68.72	85.82	76.32
DOA-GAN [20]	96.99	76.30	85.60	98.87	63.57	80.45	97.69	66.58	81.72	0.83	96.83	96.14	96.48
HiFi-Net [17]	92.80	7.10	46.00	98.80	1.90	26.00	95.30	2.50	29.00	0.52	66.00	84.00	74.00
TruFor [16]	96.88	77.10	86.42	99.01	65.92	81.93	97.99	67.82	82.89	0.85	96.95	96.88	96.59
SparseViT [38]	97.01	77.85	87.23	99.10	66.91	82.47	98.06	68.29	83.44	0.86	97.10	97.08	96.71
Forensim w/o Sim_Attn	92.62	69.43	78.67	97.11	57.64	72.56	96.23	61.36	74.69	0.78	86.95	81.67	80.06
Forensim w/o MSSA	91.48	68.87	77.39	96.81	58.35	71.43	95.75	60.84	72.91	0.77	85.94	80.62	79.48
Forensim w/o Detection	<u>97.23</u>	<u>78.43</u>	<u>88.63</u>	98.91	<u>68.92</u>	<u>82.64</u>	<u>98.11</u>	<u>69.37</u>	82.14	0.88	<u>97.22</u>	<u>97.38</u>	<u>96.84</u>
<b>Forensim</b>	<b>97.43</b>	<b>79.61</b>	<b>89.29</b>	<b>99.34</b>	<b>70.49</b>	<b>99.67</b>	<b>99.92</b>	<b>74.83</b>	<b>84.48</b>	<b>0.90</b>	<b>98.47</b>	<b>97.64</b>	<b>96.98</b>
<b>CMFD Anything Test Set (Ours)</b>													
BusterNet [46]	47.34	36.88	35.16	53.42	26.78	34.96	47.87	28.34	31.26	0.47	44.56	42.61	43.12
ManTra-Net [47]	48.65	7.16	37.48	64.98	2.21	24.85	48.16	2.41	27.89	0.44	52.62	64.93	57.14
DOA-GAN [20]	53.48	48.72	52.67	61.83	32.12	43.74	73.36	37.62	44.83	0.60	70.06	73.44	71.42
HiFi-Net [17]	47.50	6.50	36.00	73.00	1.90	23.00	47.20	2.10	26.00	0.43	51.00	63.00	55.50
TruFor [16]	56.91	50.83	57.63	65.42	36.21	47.32	77.83	41.29	49.51	0.63	72.45	74.62	73.01
SparseViT [38]	57.74	52.14	59.95	67.88	38.04	49.89	79.36	43.16	51.73	0.65	73.12	75.81	74.16
Forensim w/o Sim_Attn	52.68	47.39	50.64	58.19	30.87	43.26	70.83	35.87	41.27	0.58	67.58	68.92	66.84
Forensim w/o MSSA	51.67	47.18	49.21	56.82	31.58	42.96	68.12	34.59	40.26	0.57	66.89	67.14	65.72
Forensim w/o Detection	<u>58.45</u>	<u>53.72</u>	<u>61.28</u>	<u>68.76</u>	<u>40.74</u>	<u>51.96</u>	<u>81.23</u>	<u>48.73</u>	<u>53.47</u>	<u>0.68</u>	<u>74.94</u>	<u>76.83</u>	<u>75.17</u>
<b>Forensim</b>	<b>59.41</b>	<b>54.82</b>	<b>64.77</b>	<b>69.74</b>	<b>41.91</b>	<b>53.43</b>	<b>82.67</b>	<b>50.61</b>	<b>54.16</b>	<b>0.70</b>	<b>75.12</b>	<b>77.42</b>	<b>75.68</b>

Table 2. CMFD results on USC-ISI CMFD [46] and CMFD-Anything (ours) test sets. Localization uses pixel-level precision, recall, F1 (Pristine(P)/Source(S)/Target(T) regions), and AUC. Detection uses image-level metrics. **Bold** = best per column, underline = second best.

masks ([pristine](#), [source](#), [target](#)) for all manipulation types, as shown in [Fig. 6](#). Unlike prior splicing models [3, 16, 17, 25, 38, 47], which are trained with binary masks ([Fig. 5a](#)), capture only artifact cues, and do not model duplication or source regions, our proposed setup ([Fig. 5b](#)) uses 3-class supervision—even for spliced images—enabling the model to learn explicit source-target relationships. This joint modeling of Sim\_Map and MSSA\_Map allows the network to generalize across manipulation types without task-specific datasets or architectural modifications. While we do not claim to be the first to address CMFD, our key novelty lies in framing Forensim as the first general-purpose IMDL framework trained using a three-class-based training formulation, rather than targeting a specific task like splicing or copy-move. Importantly, we argue that three-class-based training is not a simplified subset of splicing; rather, localizing both source and target regions constitutes a more structured and fine-grained supervision signal than detecting tampering boundaries or artifact regions alone.

## 4.2. Motivation and Dataset Gap

As summarized in Table 1 of [30], existing CMFD benchmarks include only 941 forged images across four public datasets, none providing three-class RGB masks required to train models like Forensim. USC-ISI CMFD [46], based on MS-COCO [26] and SUN2012 [48], contains synthetic images that are often visually obvious and unrealistic. In practice, skilled adversaries can create convincing forgeries difficult to detect—even for humans. Reproducibility is also hindered as USC-ISI CMFD is no longer publicly available, and newer datasets like CatNet [25] focus only on splicing.

These limitations underscore the need for a realistic, large-scale CMFDAnything dataset.

## 4.3. CMFDAnything Dataset

We introduce CMFDAnything, a high-resolution benchmark built from SA-1B images and masks [23]. Forgeries are created via two strategies: (1) duplicating an object within single-category images, and (2) copying objects from multi-object images to form multiple variants. Each paste is refined with MGMatting [50] and mild clone-stamp-style transforms (translation, small rotation/scale). As existing CMFD datasets lack negative (pristine) samples, we include 100K unaltered images from SA-1B to enable supervised training and false-positive calibration. The final dataset has 200K forged and 100K pristine images, split 8:1:1 (train/val/test); examples are shown in [Fig. 1](#).

**Copy placement.** We select destinations in two steps: (i) axis-aligned proposals by sliding along the  $x/y$  axes through the source centroid and along its principal axis, subject to distance/scale/overlap gates; (ii) semantic filtering with OpenCLIP [5] image-only embeddings on local context windows, choosing the arg-max cosine match and requiring  $\cos \geq \tau$  (default  $\tau=0.30$ ). We will release per-instance metadata (source/target masks, transform, chosen axis, and similarity) for transparent provenance evaluation.

**Quality Assessment.** We evaluate CMFDAnything using No-Reference [41, 49] (forged-only) and Full-Reference [43, 51] (forged vs. pristine) metrics. As shown in [Tab. 1](#), it outperforms CASIA [10] and CoMoFoD [39]. To filter low-quality forgeries, we train a binary classifier to reject synthetic samples that are easily identified as fake.

Table 3. Pixel and Image-level on CASIA and CoMoFoD CMFD datasets. **Bold = Best**, Underline = Second-Best.

Method	Localization			AUC (Loc.)	Detection		
	Prec.	Rec.	F1		Prec.	Rec.	F1
<b>CASIA CMFD [10]</b>							
BusterNet [46]	42.15	30.54	33.72	0.38	48.34	75.12	58.82
ManTraNet [47]	38.12	27.42	30.85	0.32	52.13	67.14	58.76
DOA-GAN [20]	54.70	39.67	41.44	0.46	63.39	77.00	69.53
TruFor [16]	<u>55.67</u>	41.83	43.62	<u>0.47</u>	78.92	86.32	82.43
SparseViT [38]	54.32	<u>42.91</u>	<u>45.87</u>	0.46	77.81	<u>87.43</u>	83.23
<b>Forensim</b>	<b>61.87</b>	<b>47.24</b>	<b>58.12</b>	<b>0.57</b>	<b>84.24</b>	<b>91.71</b>	<b>89.12</b>
w/o Sim_Attn	54.78	41.42	42.91	0.46	77.42	85.03	80.92
w/o MSSA	54.32	40.87	42.48	0.45	77.23	84.87	80.76
<b>CoMoFoD CMFD [39]</b>							
BusterNet [46]	51.25	28.20	35.34	0.39	53.20	57.41	55.22
ManTraNet [47]	36.11	25.48	28.34	0.30	50.34	54.92	52.48
DOA-GAN [20]	48.42	37.84	36.92	0.42	60.38	65.98	63.05
TruFor [16]	49.83	<u>38.74</u>	36.54	<u>0.43</u>	66.91	<u>71.25</u>	68.94
SparseViT [38]	<u>51.15</u>	37.20	37.92	0.42	67.70	70.41	69.83
<b>Forensim</b>	<b>56.41</b>	<b>43.57</b>	<b>47.82</b>	<b>0.51</b>	<b>76.58</b>	<b>77.94</b>	<b>75.82</b>
w/o Sim_Attn	49.51	36.83	35.91	0.41	66.35	69.01	67.31
w/o MSSA	48.89	36.20	35.47	0.40	66.02	68.74	67.10

#### 4.4. Training and Implementation

Images are resized to  $224 \times 224$  and processed with a DINO-pretrained Vision Transformer backbone. Models are implemented in PyTorch and trained on an NVIDIA RTX A5000 GPU using AdamW (batch size 64). A cyclic learning rate ( $1 \times 10^{-3}$  to  $1 \times 10^{-5}$ ) is used with StepLR decay (0.5 every 10 epochs). Early stopping is applied based on validation loss. Forensim is trained for 100 epochs on 100K randomly sampled images per epoch from the training pool. The model is optimized with Cross-Entropy and InfoNCE losses, with additional trials using Dice and Focal losses to mitigate class imbalance (details in supplementary).

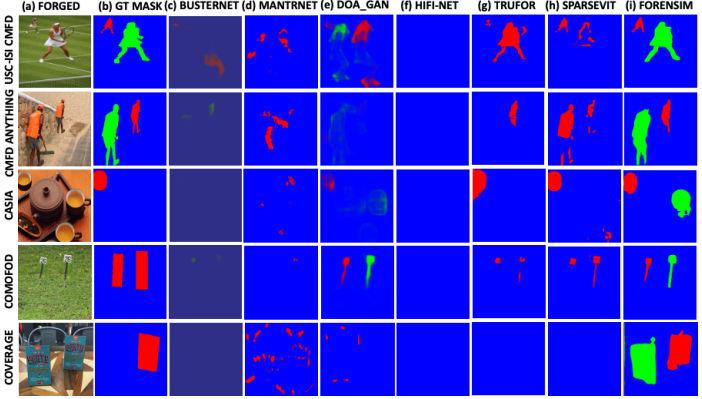
### 5. Experimental Evaluation

#### 5.1. Evaluation Datasets and Metrics

We evaluate Forensim on three standard copy-move forgery detection (CMFD) benchmarks—USC-ISI CMFD [46], CoMoFoD [39], and CASIA CMFD [10]—as well as the test split of our proposed CMFDAnything dataset. Additionally, we assess generalization on four tampered image detection and localization (IMDL) datasets: NIST16 [1], Columbia [31], Coverage [44], and CASIA [10]. Notably, neither CASIA nor CoMoFoD provides source and target masks—only binary annotations (red pixels in Fig. 6).

For evaluation, we report both pixel-level and image-level metrics. Pixel-level performance is assessed using precision, recall, F1-score, and AUC across three forgery classes: **pristine**, **source**, and **target**, derived from three-class RGB masks generated by Forensim and baseline methods. Image-level detection is evaluated using precision, recall, and F1-score. To ensure consistent global evaluation, true positives (TP), false positives (FP), and false negatives (FN) are aggregated across the entire dataset prior to metric computation. Following prior works [20, 46, 47], we apply a 200-pixel threshold (for  $320 \times 320$  images) to suppress small false positives.

Figure 6. Qualitative results on four CMFD datasets. Rows:Datasets; Columns:Models. Zoom in to view Untampered, Source, Target.



Tab. 2 and Tab. 3 present detailed pixel- and image-level results on CMFD datasets. Tab. 4 reports pixel-level F1 scores across four IMLD benchmarks, highlighting the generalization of Forensim to diverse manipulation types and real-world forgeries.

#### 5.2. Forensim Results and Analysis

For fairness and reproducibility, we restrict comparisons to models with publicly accessible code. All baseline methods were retrained following the protocol in [25] and evaluated on publicly available benchmark datasets. We compare Forensim against models trained on binary masks across both CMFD-specific and IMLD datasets, validating the effectiveness of our three-class training formulation. As shown in Tab. 2, Tab. 3, and Tab. 4, Forensim consistently achieves the best F1 and AUC scores for both pixel-level localization and image-level detection across all benchmarks.

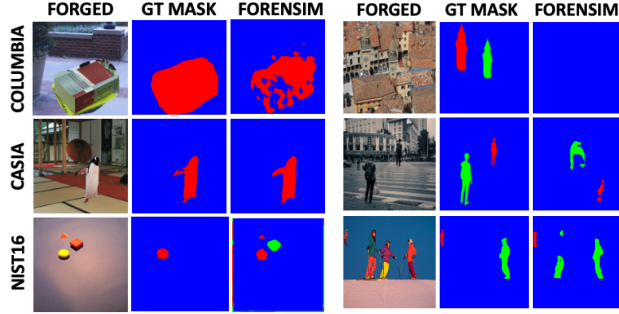
Forensim independently models duplication similarity (Sim\_Map) and manipulation structure (MSSA\_Map), subsequently refined through non-local aggregation. It outputs three-class source-target masks—outperforming SOTA IMLD baselines in qualitative evaluation (Fig. 6) and outputs binary forgery masks for splicing, when no in-image source exists (Fig. 7a). Despite its strong performance, Forensim remains efficient—36.7M params and 28.7 GFLOPs at  $512 \times 512$  resolution, while outperforming larger baselines like TruFor [16], SparseViT [38] (Tab. 7).

#### 5.3. Ablation Analysis and Robustness

We perform ablations on three Forensim components: Sim\_Attn, MSSA, and the detection branch (Tab. 2, Tab. 3). To further understand key design choices, we analyze normalization strategies and pre-processing conditions. Tab. 5 shows pixel-level F1 scores across three variants of the Sim\_Attn normalization. The BiSoftmax configuration, which applies full normalization along both row and column dimensions, consistently outperforms the raw and Row-only variants across datasets. This demonstrates the

Table 4. Pixel-level F1 localization on benchmark IMDL datasets using best threshold and a fixed threshold of 0.5 following [16].

Method	NIST [1]				COL [31]				COV [44]				CASIA [10]				Avg.
	Best		Fixed		Best		Fixed		Best		Fixed		Best		Fixed		
ManTra [47]	21.9	19.3	47.5	46.2	21.1	19.6	38.2	32.7	32.2	29.5							
TruFor [16]	35.6	34.8	89.4	88.5	47.3	45.7	83.5	81.8	63.9	62.7							
SparseViT [38]	39.4	38.4	<b>95.9</b>	<b>95.9</b>	<u>52.5</u>	<u>51.3</u>	<b>84.2</b>	<b>82.7</b>	<u>68.0</u>	<u>67.1</u>							
<b>Forensim (Ours)</b>	<b>40.2</b>	<b>39.1</b>	<u>94.2</u>	<u>93.8</u>	<b>55.7</b>	<b>54.6</b>	<u>83.4</u>	<u>81.8</u>	<b>68.4</b>	<b>67.3</b>							



(a) Benchmark IMDL Localization (b) Misdetection and False Alarms

Figure 7. (a) Forensim IMDL; (b) Forensim Limitations

importance of bi-directional affinity normalization for capturing discriminative similarity cues in IMDL.

Tab. 6 presents additional ablations on the CMFDAnything benchmark by varying mask generation strategies. Removing the MGMatting post-processing, replacing three-class masks with binary masks, or introducing noise into ground truth annotations each lead to degraded performance across all input resolutions. In contrast, the full CMFDAnything pipeline achieves the best F1 scores, particularly at  $512 \times 512$ , highlighting the value of high-fidelity soft masks and precise annotations for robust model training.

To assess robustness, we test Forensim under six perturbations—brightness, JPEG compression, contrast, cropping, noise, and blur—following [46, 47], plus four social-media perturbations (supplementary, Table 4) following [45]. As shown in Fig. 8, Forensim consistently outperforms state of the art across all perturbations.

These results underscore Forensim’s design: Sim\_Attn captures global duplication, MSSA local artifacts, and multi-scale state-space attention enhances robustness; with three-class supervision, Forensim demonstrates strong generalization across forgery types and image-level distortions.

#### 5.4. Failure Cases and Future Directions

While Forensim is robust overall, we observe three recurring failure modes: (i) background-matching splices where low contrast suppresses MSSA<sub>map</sub> (row 1, Fig. 7b); (ii) repetitive structures causing many-to-many matches in Aff<sub>final</sub> (row 3); and (iii) rare errors on low-color/monochrome images. Remedies include a lightweight

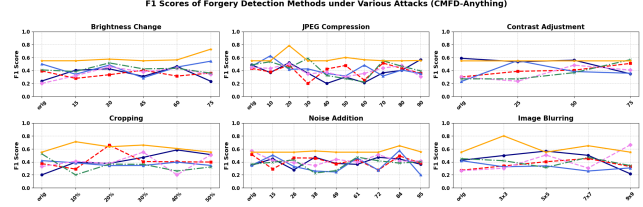


Figure 8. Robustness under attacks on CMFDAnything.

Table 5. Pixel-level F1 across normalization types in Sim\_Attn.

Variant	Norm.	CASIA CMFD [10]	CoMoFoD [39]	CMFDAnything
None	Raw	31.6	29.2	33.8
Row-only	Partial	<u>44.8</u>	<u>36.7</u>	54.3
BiSoftmax	Full	<b>58.1</b>	<u>47.8</u>	<b>62.4</b>

Table 6. Ablation studies on CMFDAnything using Forensim.

Ablation Condition	$224 \times 224$	$256 \times 256$	$320 \times 320$	$512 \times 512$
No MGMatting	56.6	57.7	58.5	61.2
Binary Mask	53.9	55.2	56.3	59.4
Noisy Groundtruth	53.4	54.6	55.5	58.4
<b>CMFDAnything</b>	<b>59.6</b>	<b>60.8</b>	<b>62.1</b>	<b>62.4</b>

Table 7. Model complexity w.r.to Resolution, Parameters, FLOPs.

Method	Backbone	Input Size	Params	FLOPs
BusterNet [46]	VGG	$256 \times 256$	15.5M	45.7G
ManTraNet [47]	VGG	$256 \times 256$	3.9M	274.0G
DOA_GAN [20]	VGG	$256 \times 256$	26.9M	46.7G
TruFor [16]	ViT	$512 \times 512$	68.7M	236.5G
SparseViT [38]	ViT	$512 \times 512$	50.3M	46.2G
<b>Forensim (Ours)</b>	SSM	$512 \times 512$	36.7M	28.7G

frequency/boundary head and photometric/codec augmentations for (i); uniqueness constraints (entropy-based or non-max suppression) and hard-negative mining for (ii); and grayscale-focused augmentation with contrast-limited adaptive histogram equalization plus a luminance similarity head for (iii). We will broaden 2D RoPE and extend to video IMDL with spatio-temporal consistency.

## 6. Conclusion

We presented Forensim, a unified framework for IMDL that accurately localizes both source and forged regions using three-class supervision. We propose similarity and manipulation attention modules within a state-space framework, enabling efficient modeling of long-range dependencies with linear complexity. Forensim addresses key limitations of existing CMFD and splicing models, which typically rely on binary masks and artifact-based cues. To support robust training and evaluation, we introduced CMFDAnything, a high-resolution dataset containing realistic copy-move forgeries. Extensive experiments across multiple benchmarks demonstrate that Forensim achieves state-of-the-art performance and generalizes effectively across manipulation types and attack scenarios, establishing it as a unified and interpretable solution for image forensics.

## References

- [1] Nimble challenge 2017 evaluation — nist. <https://www.nist.gov/itl/iad/mig/nimble-challenge-2017-evaluation>. (Accessed on 11/14/2020). 7, 8
- [2] Belhassen Bayar and Matthew C Stamm. A deep learning approach to universal image manipulation detection using a new convolutional layer. In *Proceedings of the 4th ACM workshop on information hiding and multimedia security*, pages 5–10, 2016. 2
- [3] Xinru Chen, Chengbo Dong, Jiaqi Ji, Juan Cao, and Xirong Li. Image manipulation detection by multi-view multi-scale supervision. In *Proceedings of the IEEE/CVF International Conference on Computer Vision*, pages 14185–14193, 2021. 2, 6
- [4] Jiaxin Cheng, Yue Wu, Wael AbdAlmageed, and Premkumar Natarajan. Qatm: Quality-aware template matching for deep learning. In *Proceedings of the IEEE/CVF Conference on Computer Vision and Pattern Recognition (CVPR)*, 2019. 4
- [5] Mehdi Cherti, Romain Beaumont, Ross Wightman, Mitchell Wortsman, Gabriel Ilharco, Cade Gordon, Christoph Schuhmann, Ludwig Schmidt, and Jenia Itsev. Reproducible scaling laws for contrastive language-image learning. In *CVPR*, pages 2818–2829, 2023. 6
- [6] Riccardo Corvi, Davide Cozzolino, Giada Zingarini, Giovanni Poggi, Koki Nagano, and Luisa Verdoliva. On the detection of synthetic images generated by diffusion models. In *ICASSP 2023-2023 IEEE International Conference on Acoustics, Speech and Signal Processing (ICASSP)*, pages 1–5. IEEE, 2023. 1
- [7] Davide Cozzolino, Giovanni Poggi, and Luisa Verdoliva. Efficient dense-field copy–move forgery detection. *IEEE Transactions on Information Forensics and Security*, 10(11): 2284–2297, 2015. 2
- [8] Davide Cozzolino, Giovanni Poggi, and Luisa Verdoliva. Splicebuster: A new blind image splicing detector. In *2015 IEEE International Workshop on Information Forensics and Security (WIFS)*, pages 1–6. IEEE, 2015. 2
- [9] Helisa Dhamo, Azade Farshad, Iro Laina, Nassir Navab, Gregory D Hager, Federico Tombari, and Christian Rupprecht. Semantic image manipulation using scene graphs. In *Proceedings of the IEEE/CVF conference on computer vision and pattern recognition*, pages 5213–5222, 2020. 1
- [10] Jing Dong, Wei Wang, and Tieniu Tan. Casia image tampering detection evaluation database. In *2013 IEEE China Summit and International Conference on Signal and Information Processing*, pages 422–426. IEEE, 2013. 5, 6, 7, 8
- [11] Xiaoyi Dong, Jianmin Bao, Dongdong Chen, Weiming Zhang, Nenghai Yu, Lu Yuan, Dong Chen, and Baining Guo. Cswin transformer: A general vision transformer backbone with cross-shaped windows. In *Proceedings of the IEEE/CVF conference on computer vision and pattern recognition*, pages 12124–12134, 2022. 5
- [12] Pasquale Ferrara, Tiziano Bianchi, Alessia De Rosa, and Alessandro Piva. Image forgery localization via fine-grained analysis of cfa artifacts. *IEEE Transactions on Information Forensics and Security*, 7(5):1566–1577, 2012. 2
- [13] Ian Goodfellow, Jean Pouget-Abadie, Mehdi Mirza, Bing Xu, David Warde-Farley, Sherjil Ozair, Aaron Courville, and Yoshua Bengio. Generative adversarial nets. *Advances in neural information processing systems*, 27, 2014. 1
- [14] Albert Gu and Tri Dao. Mamba: Linear-time sequence modeling with selective state spaces. *arXiv preprint arXiv:2312.00752*, 2023. 3, 4
- [15] Albert Gu, Karan Goel, and Christopher Ré. Efficiently modeling long sequences with structured state spaces. *arXiv preprint arXiv:2111.00396*, 2021. 3
- [16] Fabrizio Guillaro, Davide Cozzolino, Avneesh Sud, Nicholas Dufour, and Luisa Verdoliva. Trufor: Leveraging all-round clues for trustworthy image forgery detection and localization. In *Proceedings of the IEEE/CVF Conference on Computer Vision and Pattern Recognition*, pages 20606–20615, 2023. 2, 6, 7, 8
- [17] Xiao Guo, Xiaohong Liu, Zhiyuan Ren, Steven Grosz, Iacopo Masi, and Xiaoming Liu. Hierarchical fine-grained image forgery detection and localization. In *Proceedings of the IEEE/CVF Conference on Computer Vision and Pattern Recognition*, pages 3155–3165, 2023. 2, 6
- [18] János Horváth, Sriram Baireddy, Hanxiang Hao, Daniel Mas Montserrat, and Edward J Delp. Manipulation detection in satellite images using vision transformer. In *Proceedings of the IEEE/CVF Conference on Computer Vision and Pattern Recognition*, pages 1032–1041, 2021. 1
- [19] Minyoung Huh, Andrew Liu, Andrew Owens, and Alexei A Efros. Fighting fake news: Image splice detection via learned self-consistency. In *Proceedings of the European conference on computer vision (ECCV)*, pages 101–117, 2018. 1
- [20] Ashraful Islam, Chengjiang Long, Arslan Basharat, and Anthony Hoogs. Doa-gan: Dual-order attentive generative adversarial network for image copy-move forgery detection and localization. In *Proceedings of the IEEE/CVF Conference on Computer Vision and Pattern Recognition*, pages 4676–4685, 2020. 3, 6, 7, 8
- [21] Rudolph Emil Kalman. A new approach to linear filtering and prediction problems. 1960. 3
- [22] Diederik P Kingma and Max Welling. Auto-encoding variational bayes. *arXiv preprint arXiv:1312.6114*, 2013. 1
- [23] Alexander Kirillov, Eric Mintun, Nikhila Ravi, Hanzi Mao, Chloe Rolland, Laura Gustafson, Tete Xiao, Spencer Whitehead, Alexander C Berg, Wan-Yen Lo, et al. Segment anything. *arXiv preprint arXiv:2304.02643*, 2023. 2, 6
- [24] Neal Krawetz and Hacker Factor Solutions. A picture’s worth. *Hacker Factor Solutions*, 6(2):2, 2007. 2
- [25] Myung-Joon Kwon, In-Jae Yu, Seung-Hun Nam, and Heung-Kyu Lee. Cat-net: Compression artifact tracing network for detection and localization of image splicing. In *Proceedings of the IEEE/CVF Winter Conference on Applications of Computer Vision*, pages 375–384, 2021. 2, 6, 7
- [26] Tsung-Yi Lin, Michael Maire, Serge Belongie, James Hays, Pietro Perona, Deva Ramanan, Piotr Dollár, and C Lawrence Zitnick. Microsoft coco: Common objects in context. In *Computer Vision–ECCV 2014: 13th European Conference, Zurich, Switzerland, September 6–12, 2014, Proceedings, Part V 13*, pages 740–755. Springer, 2014. 2, 3, 6

[27] Yue Liu, Yunjie Tian, Yuzhong Zhao, Hongtian Yu, Lingxi Xie, Yaowei Wang, Qixiang Ye, and Yunfan Liu. Vmamba: Visual state space model. *arXiv preprint arXiv:2401.10166*, 2024. 3

[28] Babak Mahdian and Stanislav Saic. Using noise inconsistencies for blind image forensics. *Image and Vision Computing*, 27(10):1497–1503, 2009. 2

[29] Mehdi Mirza and Simon Osindero. Conditional generative adversarial nets. *arXiv preprint arXiv:1411.1784*, 2014. 1

[30] Soumyaroop Nandi, Prem Natarajan, and Wael Abd-Almageed. Trainfors: A large benchmark training dataset for image manipulation detection and localization. In *Proceedings of the IEEE/CVF International Conference on Computer Vision*, pages 403–414, 2023. 6

[31] Tian-Tsong Ng, Jessie Hsu, and Shih-Fu Chang. Columbia image splicing detection evaluation dataset. *DVMM lab, Columbia Univ CalPhotos Digit Libr*, 2009. 7, 8

[32] Taesung Park, Jun-Yan Zhu, Oliver Wang, Jingwan Lu, Eli Shechtman, Alexei Efros, and Richard Zhang. Swapping autoencoder for deep image manipulation. *Advances in Neural Information Processing Systems*, 33:7198–7211, 2020. 1

[33] Yunchen Pu, Zhe Gan, Ricardo Henao, Xin Yuan, Chun-yuan Li, Andrew Stevens, and Lawrence Carin. Variational autoencoder for deep learning of images, labels and captions. *Advances in neural information processing systems*, 29, 2016. 1

[34] Ekraam Sabir, Jiaxin Cheng, Ayush Jaiswal, Wael AbdAlmageed, Iacopo Masi, and Prem Natarajan. Recurrent convolutional strategies for face manipulation detection in videos. *Interfaces (GUI)*, 3(1):80–87, 2019. 1

[35] Ekraam Sabir, Soumyaroop Nandi, Wael Abd-Almageed, and Prem Natarajan. Biofors: A large biomedical image forensics dataset. In *Proceedings of the IEEE/CVF International Conference on Computer Vision*, pages 10963–10973, 2021. 1

[36] Ekraam Sabir, Soumyaroop Nandi, Wael AbdAlmageed, and Prem Natarajan. Monet: Multi-scale overlap network for duplication detection in biomedical images. In *2022 IEEE International Conference on Image Processing (ICIP)*, pages 3793–3797. IEEE, 2022. 1

[37] Jianlin Su, Murtadha Ahmed, Yu Lu, Shengfeng Pan, Wen Bo, and Yunfeng Liu. Rofomer: Enhanced transformer with rotary position embedding. *Neurocomputing*, 568:127063, 2024. 4, 5

[38] Lei Su, Xiaochen Ma, Xuekang Zhu, Chaoqun Niu, Zeyu Lei, and Ji-Zhe Zhou. Can we get rid of handcrafted feature extractors? sparsevit: Nonsemantics-centered, parameter-efficient image manipulation localization through sparse-coding transformer. In *Proceedings of the AAAI Conference on Artificial Intelligence*, pages 7024–7032, 2025. 6, 7, 8

[39] Dijana Tralic, Ivan Zupancic, Sonja Grgic, and Mislav Grgic. Comofod—new database for copy-move forgery detection. In *Proceedings ELMAR-2013*, pages 49–54. IEEE, 2013. 5, 6, 7, 8

[40] Yael Vinker, Eliahu Horwitz, Nir Zabari, and Yedid Hoshen. Deep single image manipulation. *arXiv preprint arXiv:2007.01289*, 2020. 1

[41] Jianyi Wang, Kelvin CK Chan, and Chen Change Loy. Exploring clip for assessing the look and feel of images. In *Proceedings of the AAAI conference on artificial intelligence*, pages 2555–2563, 2023. 5, 6

[42] Sheng-Yu Wang, Oliver Wang, Richard Zhang, Andrew Owens, and Alexei A Efros. Cnn-generated images are surprisingly easy to spot... for now. In *Proceedings of the IEEE/CVF conference on computer vision and pattern recognition*, pages 8695–8704, 2020. 1

[43] Zhou Wang, Alan C Bovik, Hamid R Sheikh, and Eero P Simoncelli. Image quality assessment: from error visibility to structural similarity. *IEEE transactions on image processing*, 13(4):600–612, 2004. 5, 6

[44] Bihan Wen, Ye Zhu, Ramanathan Subramanian, Tian-Tsong Ng, Xuanjing Shen, and Stefan Winkler. Coverage—a novel database for copy-move forgery detection. In *2016 IEEE International Conference on Image Processing (ICIP)*, pages 161–165. IEEE, 2016. 7, 8

[45] Haiwei Wu, Jiantao Zhou, Jinyu Tian, Jun Liu, and Yu Qiao. Robust image forgery detection against transmission over online social networks. *IEEE Transactions on Information Forensics and Security*, 17:443–456, 2022. 1, 2, 8

[46] Yue Wu, Wael AbdAlmageed, and Prem Natarajan. Buster-net: Detecting copy-move image forgery with source/target localization. In *Proceedings of the European conference on computer vision (ECCV)*, pages 168–184, 2018. 3, 6, 7, 8

[47] Yue Wu, Wael AbdAlmageed, and Premkumar Natarajan. Mantra-net: Manipulation tracing network for detection and localization of image forgeries with anomalous features. In *Proceedings of the IEEE/CVF Conference on Computer Vision and Pattern Recognition*, pages 9543–9552, 2019. 2, 6, 7, 8

[48] Jianxiong Xiao, James Hays, Krista A Ehinger, Aude Oliva, and Antonio Torralba. Sun database: Large-scale scene recognition from abbey to zoo. In *2010 IEEE computer society conference on computer vision and pattern recognition*, pages 3485–3492. IEEE, 2010. 3, 6

[49] Zhenqiang Ying, Haoran Niu, Praful Gupta, Dhruv Mahajan, Deepthi Ghadiyaram, and Alan Bovik. From patches to pictures (paq-2-piq): Mapping the perceptual space of picture quality. In *Proceedings of the IEEE/CVF conference on computer vision and pattern recognition*, pages 3575–3585, 2020. 5, 6

[50] Qihang Yu, Jianming Zhang, He Zhang, Yilin Wang, Zhe Lin, Ning Xu, Yutong Bai, and Alan Yuille. Mask guided matting via progressive refinement network. In *Proceedings of the IEEE/CVF Conference on Computer Vision and Pattern Recognition*, pages 1154–1163, 2021. 6

[51] Richard Zhang, Phillip Isola, Alexei A Efros, Eli Shechtman, and Oliver Wang. The unreasonable effectiveness of deep features as a perceptual metric. In *Proceedings of the IEEE conference on computer vision and pattern recognition*, pages 586–595, 2018. 5, 6

[52] Jun-Yan Zhu, Taesung Park, Phillip Isola, and Alexei A Efros. Unpaired image-to-image translation using cycle-consistent adversarial networks. In *Proceedings of the IEEE international conference on computer vision*, pages 2223–2232, 2017. 1

- [53] Lianghui Zhu, Bencheng Liao, Qian Zhang, Xinlong Wang, Wenyu Liu, and Xinggang Wang. Vision mamba: Efficient visual representation learning with bidirectional state space model. *arXiv preprint arXiv:2401.09417*, 2024. [3](#)
- [54] Xinshan Zhu, Yongjun Qian, Xianfeng Zhao, Biao Sun, and Ya Sun. A deep learning approach to patch-based image inpainting forensics. *Signal Processing: Image Communication*, 67:90–99, 2018. [2](#)